Published in final edited form as:
Curr Pharm Biotechnol. 2012 June ; 13(7): 1332–1345.

Ultrasound-Induced Blood-Brain Barrier Opening

Elisa E. Konofagou[a,b,*], **Yao-Sheng Tung**[a], **James Choi**[a], **Thomas Deffieux**[a], **Babak Baseri**[a], and **Fotios Vlachos**[a]

[a]Department of Biomedical Engineering, Columbia University, New York, NY, USA

[b]Department of Radiology, Columbia University, New York, NY, USA

Abstract

Over 4 million U.S. men and women suffer from Alzheimer's disease; 1 million from Parkinson's disease; 350,000 from multiple sclerosis (MS); and 20,000 from amyotrophic lateral sclerosis (ALS). Worldwide, these four diseases account for more than 20 million patients. In addition, aging greatly increases the risk of neurodegenerative disease. Although great progress has been made in recent years toward understanding of these diseases, few effective treatments and no cures are currently available. This is mainly due to the impermeability of the blood-brain barrier (BBB) that allows only 5% of the 7000 small-molecule drugs available to treat only a tiny fraction of these diseases. On the other hand, safe and localized opening of the BBB has been proven to present a significant challenge. Of the methods used for BBB disruption shown to be effective, Focused Ultrasound (FUS), in conjunction with microbubbles, is the only technique that can induce localized BBB opening noninvasively and regionally. FUS may thus have a huge impact in trans-BBB brain drug delivery. The primary objective in this paper is to elucidate the interactions between ultrasound, microbubbles and the local microenvironment during BBB opening with FUS, which are responsible for inducing the BBB disruption. The mechanism of the BBB opening *in vivo* is monitored through the MRI and passive cavitation detection (PCD), and the safety of BBB disruption is assessed using H&E histology at distinct pressures, pulse lengths and microbubble diameters. It is hereby shown that the BBB can be disrupted safely and transiently under specific acoustic pressures (under 0.45 MPa) and microbubble (diameter under 8 μm) conditions.

Keywords

Blood-brain barrier; brain drug delivery; disruption; focused ultrasound; microbubble; safety

INTRODUCTION

Current treatments of neurological and neurodegenerative diseases are limited due to the lack of a truly noninvasive, transient, and regionally selective brain drug delivery method

*Address correspondence to this author at the Department of Radiology, Columbia University, New York, NY, USA; ek2191@columbia.edu.

CONFLICT OF INTEREST
None declared.

[1]. The brain is particularly difficult to deliver drugs to because of the blood-brain barrier (BBB). The impermeability of the BBB is due to tight junctions connecting adjacent endothelial cells and highly regulatory transport systems of the endothelial cell membranes [2]. The main function of the BBB is ion and volume regulation in order to ensure conditions necessary for proper synaptic and axonal signaling [3]. However, the same impermeability properties that keep the brain healthy are the reason for the difficulties in its efficient pharmacological treatment. The BBB prevents most neurologically active drugs from entering the brain, and, as a result, has been determined as the rate-limiting factor in brain drug delivery [1]. Until a solution to the trans-BBB delivery problem is found, treatments of neurological diseases will remain impeded.

THE BLOOD-BRAIN BARRIER (BBB) PHYSIOLOGY: STRUCTURE AND FUNCTION

The BBB is a specialized substructure of the vascular system consisting of endothelial cells connected together by tight junctions. The luminal and abluminal membranes line the inner wall of the vessel and act as the permeability barrier. The combination of tight junctions and these two membranes characterizes the BBB as having low permeability to large and ionic substances. However, certain molecules such as glucose and amino acids are exceptions, because they are actively transported. It has also been shown that lymphocytes can traverse the BBB by going through temporarily opened tight junctions of the endothelial walls. The astrocytes have been proven to offer a protective mechanism of the neurons to any mechanical effect [2].

THE BBB AND NEUROTHERAPEUTICS

Several neurological disorders remain intractable to treatment by therapeutic agents because of the BBB, the brain's natural defense. By acting as a permeability barrier, the BBB impedes entry from blood to the brain of virtually all molecules with higher than 400 Da of molecular weight Fig. (**1**), thus rendering many potent neurologically active substances and drugs ineffective simply because they cannot be delivered to where they are needed. As a result, traversing the BBB remains the rate-limiting factor in brain drug delivery development [1].

FOCUSED ULTRASOUND (FUS)

Focused ultrasound (FUS) utilizes the same concept of acoustic wave propagation as the more widely known diagnostic ultrasound applications. However, instead of acquiring and displaying echoes generated at several tissue interfaces for imaging, FUS employs concave transducers that usually have a single geometric focus, at which most of the power is delivered during sonication in order to induce mechanical effects, thermal effects, or both. Note that the more widely used ‘High-Intensity Focused Ultrasound (HIFU)’ name of the method is not used here for BBB opening since the intensities used are low, i.e., on the level of what is used in diagnostic ultrasound.

BBB OPENING USING FUS AND MICROBUBBLES

Blood-brain barrier opening induced by ultrasound at or near ablation intensities was first observed while accompanied by neuronal damage [5-8]. After reducing the acoustic intensity and duty cycle, BBB opening was still observed, but without the macroscopic damage detected as lesions [9]. With the addition of intravenously(IV)-injected microbubbles prior to sonication, BBB opening was determined to be transient [10] in the presence of Optison™ (Optison™; Mallinckrodt Inc., St. Louis, MO), which are albumin-coated, octafluoropropane-filled microbubbles of 3-4.5 μm in diameter and are usually used to enhance blood vessels on clinical ultrasound images through opacification. The BBB opening procedure could also be monitored with MRI and MR contrast agents [10]. This showed the potential of opening the BBB without damaging parenchymal cells, such as neurons. Further investigation entailed study of this phenomenon with Optison™ to search for a difference in threshold of BBB opening and neuronal damage and understand the mechanism of the opening in rabbits, with [11-13] or without [14] a craniotomy. The advantage of having microbubbles present in the blood supply is that it allows for the reduction of the ultrasound intensity, the containment of most of the disruption within the vasculature, and the reduction of the likelihood of irreversible neuronal damage [11-21]. Although there are many indications that damage can be contained to minimal hemorrhage [16], the complete safety profile remains to be assessed. In addition, indications to various mechanisms such as the dilation of vessels, temporary ischemia, mechanically induced opening of the tight junctions, and the activation of various transport mechanisms have been reported [9, 13, 18].

Our group has demonstrated feasibility of BBB opening through the intact skull and scalp and successful imaging of the BBB opening in the area of the hippocampus at sub-millimeter imaging resolution using a 9.4T MR scanner in both wildtype [19, 21-23] and Alzheimer's mice [24]. Our group also concentrates on a specific brain region (e.g., the hippocampus), which is key in neurodegenerative disease, such as Alzheimer's, and can be successfully and reproducibly targeted [25]. Delivery of molecules of up to 2000 kDa in molecular weight was also demonstrated [26]. Preliminary histology indicated no structural damage in the area of the hippocampus [27]. Finally, it is important to note that the microbubbles used for BBB opening have been approved by the Food and Drug Administration (FDA) for human use in contrast echocardiography, e.g., for the detection of myocardial infarction [28]. It is equally important to specify that the pressure amplitudes used for BBB opening are of similar range to ultrasound diagnostic levels (<1.5-2 MPa) and, therefore, assumed safe for human use [29] while the pulse duration can be by orders of magnitude longer.

MICROBUBBLES IN CONTRAST ULTRASOUND AND ASSOCIATED BIOEFFECTS

Currently, in the U.S., microbubbles are only FDA-approved for echocardiography in patients with sub-optimal images of the cardiac chambers. However, microbubbles have shown promise for imaging myocardial perfusion using intermittent contrast destruction pulses. Therefore, most *in vivo* bioeffects studies have focused on the heart [30]. For a given

frequency, separate pressure thresholds exist for microbubble destruction and the onset of bioeffects [31-33]. Safe cardiac perfusion imaging would then be done with the microbubble clearance pulse being between these thresholds. Extravascular drug delivery to the brain would then be performed near the threshold for transient opening, but well below the conditions for permanent damage. Human doses for commercially available microbubbles used in contrast echocardiography could provide a useful benchmark for therapy trials. However, the human dose for imaging purposes varies widely (Table **1**). A typical dose ranges between 6-12 × 10^7 microbubbles per kg (60-120 microbubbles per mg). Mean diameters are given, but detailed information of the polydispersed size distributions is lacking. Thus, the effects of microbubble size and concentration on safety are difficult to decouple from previous studies using these commercial agents. Our ability to generate and isolate microbubbles of distinct and narrow size distributions with well defined concentrations will allow us to probe these effects in the proposed study.

Several studies have shown an increase in bioeffects with increasing microbubble dose. For Definity and Optison, increases in rat cardiomyocyte cell death, premature heart beats and microvessel leakage were found after insonation [33, 37]. Similar dose-response relationships have been observed for BBB opening [34, 35], Yang, [37] compared insonation of Optison, Definity and Imagent in the rat heart and found that microvascular effects were similar when expressed as the number of microbubbles injected. They concluded that shell type and encapsulated gas have little effect on bioeffects. Given the polydispersed size distribution of the different formulations, however, the effects of size are difficult to glean from that study. However, little is known about the effects of microbubble size on bioeffects. Christiansen *et al.,* [38] found that intra-arterial injection was more effective than intravenous injection for gene transfection through sonoporation. This result was attributed to the difference in microbubble sizes delivered to the insonified region. Several biophysical studies have shown remarkable size dependence for microbubble oscillation and destruction [39, 40].

CLINICAL RELEVANCE OF BBB DISRUPTION

Neurodegenerative Disease

Over 4 million U.S. men and women suffer from Alzheimer's disease; 1 million from Parkinson's disease; 350,000 from multiple sclerosis; and 20,000 from ALS. Worldwide, these four diseases account for more than 20 million patients. Although great progress has been made in recent years toward understanding of neurodegenerative diseases like Alzheimer's, Parkinson's, multiple sclerosis, ALS and others, few effective treatments and no cures are currently available. Aging greatly increases the risk of neurodegenerative disease and the average age of Americans is steadily increasing. Today, over 35 million Americans are over the age of 65. Within the next 30 years this number is likely to double, putting more and more people at increased risk of neurodegenerative disease.

Alzheimer's disease, which has emerged as one of the most common brain disorders, begins in the hippocampal formation and gradually spreads to the remaining brain at its most advanced stages, and is characterized partly by deposition of amyloid plaques in the brain tissue but also in the blood vessels themselves [41]. For the purpose of this study, we will

focus on the treatment of Alzheimer's disease through the FUS-induced blood-brain barrier opening and therefore, the targeted region in the brain will be the hippocampus.

Drug Delivery in Neurodegenerative Disease

Over the past decade, numerous small- and large-molecule products have been developed for treatment of neurodegenerative diseases with mixed success. When administered systemically *in vivo*, the BBB inhibits their delivery to the regions affected by those diseases. A review of the Comprehensive Medicinal Chemistry database indicates that only 5% of the more than 7000 small-molecule drugs treat the Central Nervous System (CNS) [4]. With these, only four CNS disorders can be treated: depression, schizophrenia, epilepsy, and chronic pain [42, 43] . Despite the availability of pharmacological agents, potentially devastating CNS disorders and age-related neurodegenerative diseases, such as Alzheimer's disease, Parkinson's disease, Huntington's disease, multiple sclerosis, and amythrophic lateral sclerosis (ALS), remain undertreated mainly because of the impermeability of the BBB [1, 4]. The goal of our studies is thus to optimize the FUS method and elucidate its mechanism in order to ultimately deliver therapeutics to the brain and significantly facilitate treatment of currently intractable and devastating neurodegenerative diseases.

A successful drug delivery system requires transient, localized, and noninvasive targeting of a specific tissue region. None of the current techniques clinically used, or currently under research, address these issues within the scope of the treatment of neurodegenerative diseases. As a result, the present situation in neurotherapeutics enjoys few successful treatments for most CNS disorders. Some of those routes of administration are listed in Table **2**. Several pharmaceutical companies use the technique known as “lipidization”, which is the addition of lipid groups to the polar ends of molecules to increase the permeability of the agent [44]. However, the effect is not localized as the permeability of the drug increases not only in the targeted region, but over the entire brain and body. There can thus be a limit to the amount absorbed before the side-effects become deleterious [44].

A second set of techniques under study are neurosurgically-based drug delivery methods, which involve the invasive implantation of drugs into a region by a needle [45, 46]. The drug spreads through diffusion and is localized to the targeted region, but diffusion does not allow for molecules to travel far from their point of release. In addition to this, invasive procedures traverse untargeted brain tissue causing unnecessary damage. As a result, effective drugs have recently been shelved after reports of adverse effects. Other techniques utilize solvents mixed with drugs or adjuvants (pharmacological agents) attached to drugs to disrupt the BBB through dilation and contraction of the blood vessels [1, 4, 47]. However, this disruption is not localized within the brain, and the solvents and adjuvants used are potentially toxic. This technique may constitute a delivery method specific to the brain, but it requires special attention to each type of drug molecule and a specific transport system resulting in a time-consuming and costly process while still not being completely localized to the targeted region. FUS in combination with microbubbles constitutes thus the only truly transient, localized, and noninvasive technique for opening the BBB. Due to these unique advantages over other existent techniques (Table **2**), FUS may facilitate the delivery of

already developed pharmacological agents and could significantly impact how CNS diseases are treated.

However, despite the fact that FUS is currently the only technique that can open the BBB locally and noninvasively, several key aspects of this phenomenon remain unexplored. A clear correlation of BBB opening with microbubbles has been shown [10, 12, 19]. Although the presence of microbubbles allows for a reduction in the necessary acoustic pressure for BBB opening, it also allows for the possibility of disrupting the microbubble through inertial cavitation [47-49]. The resulting effects can not only open the tight junctions, but also could induce irreversible damage to the blood vessels and its surrounding cells [27]. Recent studies have indicated that BBB opening may occur without necessarily incurring inertial cavitation, without [14] or with [17] craniotomy. However, it is not clear how the different types of mechanical effects lead to BBB opening and how the role of the microbubble can be optimized. Given the strong coupling of microbubble size and concentration to the response to insonation, a mechanistic study to BBB opening by contrast-assisted focused ultrasound must include these parameters. Control over both ultrasound and microbubble parameters is essential for the proper optimization and understanding of the FUS technique. However, to our knowledge, no study to date has included a thorough investigation of both of these components.

FUS-Facilitated BBB Opening in Drug Delivery for Treatment of Neurodegenerative Disease

Realizing the strong premise of this technique for facilitation of drug delivery to specific brain regions, we showed that the BBB can be opened selectively and reproducibly in the hippocampal region in mice [19-26, 50-52]. By developing a better understanding of the underlying physical parameters that are responsible for the opening of the BBB, namely, the ultrasound and microbubble parameters, we will be in a position to fully exploit this methodology and to do so safely. The feasibility of the technique at optimized ultrasound and microbubble parameters for reversible BBB opening, as determined *in vivo*, has been tested on wild-type mice as a first step to identify the potential of this technique in the treatment of neurodegenerative diseases [24]. The MR imaging methods developed allow for high sensitivity, high spatial resolution, and high temporal resolution. The latter is achieved through the slow diffusion of intraperitoneally-injected gadolinium. The added potential of combining this ultrasound technique with any therapeutic agent may renew possibilities in potentially employing available pharmacological agents, whose development has currently been abandoned because of poor BBB penetration. This may thus result in the novel and effective treatment of several, potentially devastating, neurological and neurodegenerative diseases. As indicated above, we will concentrate on the feasibility of noninvasive and localized treatment Alzheimer's disease by specifically targeting the hippocampus. However, the FUS technique can, in principle, be combined and applied in the case of any neurological disease. Therefore, findings of this study may not only impact treatment of a specific disease but also the entire field of brain diseases. In summary, FUS stands to make an important in the brain drug delivery and the proposed study aims at its optimization through understanding of the type of interaction between the microbubble, the tissue and the FUS beam.

DRUG DELIVERY THROUGH THE OPENED BBB

The delivery of many large agents using focused ultrasound (FUS) and microbubbles has been demonstrated in previous studies by our group and others: MRI contrast agents such as Omniscan (573 Da) [22] and Magnevist® (938 Da) [21], Evans Blue [53], Trypan Blue [54], Herceptin (148 kDa) [53], horseradish peroxidase (40 kDa) [55], doxorubicin (544 Da) [56], multi-sized Dextran [26] and rabbit anti-Ab antibodies [54]. Despite the promise shown by the delivery of such a variety of compounds, several questions with the effectiveness of the delivery remain. In particular, it is still not known whether therapeutic molecules can cross through the BBB opening into the intracellular neuronal space so that they can trigger the required downstream effects for neuronal regeneration [63].

METHODS FOR GENERATING AND ASSESSING BBB OPENING

FUS and Microbubbles

The experimental setup is shown in Fig. (**2**). The FUS transducer (center frequency: 1.5 MHz; focal depth: 60 mm; outer radius: 30 mm; inner radius 11.2 mm, model: cdc7411-3, Imasonic, Besançon, France) is used to perform sonication immediately following bubble administration. The transducer is driven by a function generator (Agilent Technologies, Palo Alto, CA, USA) through a 50-dB power amplifier (ENI Inc., Rochester, NY, USA). A cone filled with degassed and distilled water is attached to the transducer system. The transducer is attached to a computer-controlled positioner (Velmex Inc., Bloomfield, NY). The PCD, a 5-cm cylindrically focused broadband hydrophone (Sonic Concepts, Bothell, WA, USA), with a cylindrical focal region (height 19 mm, diameter 3.64 mm) is placed at 60^0 from the longitudinal axis of the FUS beam. The PCD and the FUS transducer are confocally aligned. The acoustic emissions from the microbubbles are captured with the PCD and collected using a digitizer (model 14200, Gage Applied Technologies, Inc., Lachine, QC, Canada) through a 20 dB amplifier (model 5800, Olympus NDT, Waltham, MA, USA). Microbubbles (Definity®: mean diameter range: 1.1-3.3 μm, Lantheus Medical Imaging, MA, USA, or lipid-shelled microbubbles manufactured in-house and size-isolated using differential centrifugation [57] are activated and used within 24 h after activation. Following activation, a 1:20 dilution solution is prepared using 1x phosphate-buffered saline (PBS) and slowly injected into the tail vein (1 μl per gram of mouse body weight). Pulsed-wave FUS (burst rate: 10 Hz; burst duration: 20 ms; duty cycle 20%) was applied. A 20-ms pulse length in two 30-s sonication intervals with a 30-s intermittent delay was used with definity while a 0.067-ms pulse length in one 60-s sonication was used with monodispersed bubbles. Peak-rarefactional acoustic pressures of 0.15, 0.30, 0.45 and 0.60 MPa are typically used as they have been shown to provide the best tradeoff between safety and BBB opening [27]. One side of the hippocampus in the horizontal orientation is sonicated in each mouse. Acoustic parameters other than the pressure have also been studied with respect to their role in BBB disruption. One of those is the pulse length [58]. In that study, mouse brains were pulse sonicated (center frequency: 1.5 MHz, peak-negative pressure: 0.51 MPa, pulse length (PL): 2.3 μs, pulse repetition frequency (PRF): 6.25, 25, 100 kHz) continuously or with a burst length of 1000 pulses (burst repetition frequency (BRF): 0.1, 1, 2, or 5 Hz) through the intact scalp and skull for 11 min. One minute after the start of sonication, fluorescence-

tagged dextran (60 μg/g, molecular weight: 3 kDa) and Definity® microbubbles (0.05 μl/g) were intravenously injected. After 20 min of circulation, the mice were transcardially perfused, and the brains were sectioned and imaged using fluorescence microscopy. In order to determine the microbubble size dependence, mice have been injected intravenously with lipid-shelled bubbles of either 1-2, 4-5 or 6-8 μm in diameter while the concentration was 10^7 numbers/mL [64].

Magnetic Resonance Imaging

A vertical-bore 9.4T MR system (Bruker Biospin, Billerica, MA, USA) was used to confirm the blood-brain barrier opening in the murine hippocampus. Each mouse was anesthetized using 1-2% of isoflurane gas and was positioned inside a single resonator. The respiration rate was monitored throughout the procedure using a monitoring or gating system (SA Instruments Inc., Stony Brook, New York, USA). Prior to introducing the mouse into the scanner, intraperitoneal (IP) catheterization was performed. Two different protocols were used for MR imaging. The first protocol was a three-dimensional (3D), T1-weighted SNAP gradient echo pulse sequence, which acquired horizontal images using TR/TE=20/4 ms, a flip angle of 25 deg, NEX of 5, a total acquisition time of 6 min and 49 s, a matrix size of 256×256×16 pixels and a field of view (FOV) of 1.92×1.92×0.5 cm^3, resulting in a resolution of 75×75×312.5 μm^3. The second protocol was a 3D T2*-weighted GEFC gradient echo pulse sequence, which acquired horizontal images using TR/TE=20/5.2 ms, a flip angle of 10 deg, NEX of 8, a total acquisition time of 8 min and 12 s, a matrix size of 256×192×16 pixels and a FOV of 2.25×1.69×0.7 cm^3, resulting in a resolution of 88×88×437.5 μm^3. Both protocols were applied approximately 30 min after IP injection of 0.30 ml of gadodiamide (590 Da, Omniscan®, GE Healthcare, Princeton, NJ, USA), which allowed sufficient time for the gadodiamide to diffuse into the sonicated region.

DCE-MRI

*T*1-weighted 2D FLASH sequence of a 192 × 128 matrix size (reconstructed to 256×128), a resolution of 130×130 μm2 (reconstructed to 98×130 μm2), a flip angle of 70 deg, TR/TE=230/3.3ms and a slice thickness of 0.6mm, with no interslice gap. The number of excitations (NEX) was equal to four and the acquisition time was 88 s.

Standard T1-Weighted Images

2D FLASH (TR/TE = 230/3.3 ms; flip angle: 70 deg; NEX = 18; scan time: 9 min 56 s; matrix size: 256×192; spatial resolution: 86×86 μm2; slice thickness: 500 μm, no interslice gap).

Acoustic Emission Signal Acquisition and Analysis

The acoustic emission signals acquired by the passive cavitation detector (PCD) are sampled at 25 MHz to accommodate the highest memory limit of the digitizer involved in each case. A customized spectrogram function (30-cycles, i.e., 20μs, Chebyshev window; 95% overlap; 4096-point FFT) in MATLAB® (2007b, Mathworks, Natick, MA) is used to generate a time-frequency map, which provided the spectral amplitude in time. The spectrogram can then clearly indicate how the frequency content of a signal changes over time. Therefore, the

onset of the broadband response and its duration could be clearly demonstrated on the spectrogram.

The acoustic emissions are quantified *in vivo*. A high-pass, Chebyshev type 1, filter with a cut-off of 4 MHz was first applied to the acquired PCD signal. The acoustic emission collected by the focused hydrophone was used in the quantification of the intertial cavitation dose (ICD), harmonic (nf, n = 1, 2, 6), sub-harmonic (f/2) and ultra-harmonics (nf/2, n = 3, 5, 7, 9) frequencies produced by stable cavitation [59] were filtered out by excluding 300-kHz bandwidths around each harmonic and 100-kHz bandwidths around each sub- and ultra-harmonic frequency. These bandwidths were designed to filter for the broadband response and to ensure that the stable cavitation response was not included in the ICD calculation. The root mean square (RMS) of the spectral amplitude (V_{RMS}) could then be obtained from the spectrogram after filtering. To maximize the broadband response compared to the sonication without microbubbles, only the first 50 μs of sonication were considered in the ICD calculation, which was performed by integrating the V_{RMS} variation within an interval of 0.75 μs (i.e., calculating the area below the V_{RMS} curve between 0.095 ms and 0.145 ms). In order to remove the effect of the skull in the ICD calculation, the V_{RMS} in the case without microbubbles was also calculated and was subtracted from the results with the microbubbles to obtain the net bubble response. A Student's *t*-test was used to determine whether the ICD was statistically different between different pressure amplitudes. A P-value of $P<0.05$ was considered to denote a significant difference in all comparisons.

ACOUSTIC PARAMETER DEPENDENCE AND MECHANISM OF BBB OPENING

The BBB opening pressure threshold is identified to fall between 0.30 and 0.45 MPa in the case of the 1-2-μm bubbles and between 0.15 and 0.30 MPa in the 4-5 and 6-8-μm cases [50, 60]. At every acoustic pressure, both the region of contrast enhancement in the MRI imaging and the amplitude of broadband emissions increased with the bubble diameter. The IC threshold is found to be bubble independent and to lie between 0.30 MPa and 0.45 MPa for all bubble sizes Fig. (**3**). In fluorescence imaging, the PL of 2.3 μs was found to be sufficient for BBB opening and Dextran delivery Fig. (**4**).

MOLECULAR DELIVERY THROUGH THE BBB OPENING

A molecular delivery study [26, 52] indicated that the range of molecular size for trans-BBB delivery spreads to well beyond the 574 Da (Gadolinium; Fig. (**3**)) to 67 KDa (Albumin; Fig. **5**) and 2000 kDa (Dextrans; Fig. (**5**)). As expected, at 2000 kDa (or, ~20 nm), the fluorescent region is the smallest (since the molecule is the largest and thus diffusion the slowest) and mostly outside of the hippocampus. Therefore, FUS-induced BBB opening was shown feasible for noninvasive, local, and transient opening of the BBB for drug delivery of agents of several tens of kDa; providing thus the opportunity of delivering available pharmacological agents to specific brain regions for treatment of neurological disease.

SAFETY AND REVERSIBILITY OF BBB OPENING

In order to determine the safety window of the FUS technique, through histological and immunohistological techniques [27], we have identified the safe operating parameters of ultrasound exposure for neurons, astrocytes, and endothelial cells Fig. (**6**). In summary, BBB opening starts occurring at 0.3 MPa rarefactional pressure amplitude and beyond. At pressures under 0.6 MPa (Fig. (**6i**)), no extravasation of red blood cells (RBC) or neuronal damage was observed in the regions of the hippocampus exhibiting the most pronounced BBB opening. Beyond 0.6 MPa (Fig. (**6ii**)), RBC extravasation was detected and beyond 0.9 MPa neuronal damage was observed. These preliminary findings suggest that there is overlap between the feasibility and safety windows within the pressure range of 0.3-0.6 MPa, i.e., the BBB can be opened throughout the entire hippocampus without endothelial or neuronal damage at those pressures Fig. (**6**); [25, 27]. FUS-induced BBB opening was reported to close within 72-hours in rabbits [10]. Fig. (**7**) shows that BBB closure had occurred within the first 24 hours after BBB opening.

PROPERTIES OF BBB OPENING

Dynamic contrast-enhanced (DCE)-MRI has been performed before and after the intraperitoneal injection of gadodiamide over 60 min [61]. The general kinetic model (GKM) is used to estimate the permeability in the entire brain [61]. At 0.3 MPa and 4-5-μm bubbles, the permeability is found to equal 0.02 ± 0.0123 min^{-1} and increase by at least 100 times in the region of BBB opening compared to the control side. Cavitation Fig. (**3**) and permeability Fig. (**8**) findings demonstrated that the inertial cavitation threshold is independent of the bubble size while both the ICD and MR signal enhancement increased at larger bubble sizes, also indicating a correlation between the cavitation and permeability increase [60]. The fact that the permeability increased with the pressure and microbubble size indicated that the BBB opening occurs at multiple sites within the capillary tree and that the BBB opening is larger with larger microbubbles, most likely due to the larger area of contact between the bubble and the capillary wall.

BBB OPENING IN LARGE ANIMALS

A 3D finite-difference, time-difference simulation platform (Wave 3000, CyberLogic, New York, USA) simulation model, validated in experiments Fig. (**7c**); [62] was used to identify the optimal frequency for successful trans-skull propagation using CT scans (GE LightSpeed Ultrafast CT of *ex vivo* non-human primate and human skulls as inputs to model absorption and speed of sound maps. The targeted brain structures were extracted from publicly available 3D brain atlases registered with the skulls (Fig. (**9a-b**)). The frequency of 500 kHz provided the best tradeoff between phase aberrations and standing wave effects in the human case while the frequency of 800 kHz was most suitable in the case of the primate skull. A fast periodic linear chirp method was developed and found capable of reducing the standing wave effects. The simple, single-element system that we have been using in mice was concluded to be feasible for BBB opening in primates and humans and the size of the focal spot dimensions fit the hippocampal sizes when targeting through the dorsal part of the skull Fig. (**9**).

THERAPEUTIC DELIVERY THROUGH THE BLOOD-BRAIN BARRIER OPENING

Neurotrophic delivery to the brain has been proven essential in reversing the neuronal degeneration process but so far has been hindered by the blood-brain barrier. In a recent study by our group, not only was it shown that the brain-derived neurotrophic factor (BDNF) can cross the ultrasound-induced blood-brain barrier opening but also that it can trigger signaling pathways in the pyramidal neurons of mice *in vivo* from the membrane to the nucleus Fig. (**10**). This opens entirely new avenues in the brain drug delivery where focused ultrasound in conjunction with microbubbles can generate downstream effects at the cellular and molecular level and thus increase the drug's efficacy and potency in controlling or reversing the disease.

CONCLUSION

The FUS in conjunction with microbubbles was hereby shown to effectively and reproducibly open the blood-brain barrier transcranially *in vivo* with its recovery occurring within the first 24 hours to a few days after depending on the parameters used. The permeability of the FUS-opened BBB was shown to increase by at least two orders of magnitude indicating facilitation of drug delivery through FUS. Molecules of a wide range in sizes were capable of traversing the opened BBB without any associated structural damage. A dependence of the BBB permeability on the pressure and the microbubble size indicated that multiple sites of BBB opening within the ultrasound beam occur simultaneously while each BBB opening site increases with the microbubble size. A new pulse sequence was designed that showed feasibility at very short pulse lengths and transcranial BBB opening in larger animals, such as non-human primates and humans, was shown feasible in simulations and *ex vivo* experiments. Finally, therapeutic molecules shown to improve the brain's cognition and aging were shown to successfully diffuse through the opened BBB but also trigger molecular effects in the various neuronal cell compartments.

Acknowledgments

This study was supported by NIH R01 EB009041, NIH R21 EY018505, NSF CAREER 0644713 and the Kinetics Foundation. The authors wish are thankful to Jameel Feshitan, M.S. and Mark Borden, PhD of the Mechanical Engineering department at University of Colorado, Boulder, for their valuable input and for providing some of the microbubbles used in the studies described.

REFERENCES

1. Pardridge WM. The blood-brain barrier: bottleneck in brain drug development. Neuro Rx. 2005; 2:3–14.
2. Abbott NJ, Ronnback L, Hansson E. Astrocyte-endothelial interactions at the blood-brain barrier. Nat Rev Neurosci. 2006; 7:41–53. [PubMed: 16371949]
3. Stewart PA, Tuor UI. Blood-eye barriers in the rat: correlation of ultrastructure with function. J. Comp. Neurol. 1994; 340:566–576. [PubMed: 8006217]
4. Pardridge WM. Molecular trojan horses for blood-brain barrier drug delivery. Discov. Med. 2006; 6:4. [PubMed: 17234121]
5. Bakay L, Ballantine HT Jr. Hueter TF, Sosa D. Ultrasonically produced changes in the blood-brain barrier. AMA Arch. Neurol. Psychiatry. 1956; 76:457–467.

6. Ballantine HT Jr. Bell E, Manlapaz J. Progress and problems in the neurological applications of focused ultrasound. J. Neurosurg. 1960; 17:858–876. [PubMed: 13686380]
7. Patrick JT, Nolting MN, Goss SA, Dines KA, Clendenon JL, Rea MA, Heimburger RF. Ultrasound and the blood-brain barrier. Adv. Exp. Med. Biol. 1990; 267:369–381. [PubMed: 2088054]
8. Vykhodtseva NI, Hynynen K, Damianou C. Histologic effects of high intensity pulsed ultrasound exposure with subharmonic emission in rabbit brain *in vivo*. Ultrasound Med. Biol. 1995; 21:969–979. [PubMed: 7491751]
9. Mesiwala AH, Farrell L, Wenzel HJ, Silbergeld DL, Crum LA, Winn HR, Mourad PD. High-intensity focused ultrasound selectively disrupts the blood-brain barrier *in vivo*. Ultrasound Med. Biol. 2002; 28:389–400. [PubMed: 11978420]
10. Hynynen K, McDannold N, Vykhodtseva N, Jolesz FA. Noninvasive MR imaging-guided focal opening of the blood-brain barrier in rabbits. Radiology. 2001; 220:640–646. [PubMed: 11526261]
11. Hynynen K, McDannold N, Vykhodtseva N, Jolesz FA. Noninvasive opening of BBB by focused ultrasound. Acta Neurochir. Suppl. 2003; 86:555–558. [PubMed: 14753505]
12. McDannold N, King RL, Hynynen K. MRI monitoring of heating produced by ultrasound absorption in the skull: *in vivo* study in pigs. Magn. Reson Med. 2004; 51:1061–1065. [PubMed: 15122691]
13. Sheikov N, McDannold N, Vykhodtseva N, Jolesz F, Hynynen K. Cellular mechanisms of the blood-brain barrier opening induced by ultrasound in presence of microbubbles. Ultrasound Med. Biol. 2004; 30:979–989. [PubMed: 15313330]
14. Hynynen K, McDannold N, Sheikov NA, Jolesz FA. Vykhodtseva N. Local and reversible blood-brain barrier disruption by noninvasive focused ultrasound at frequencies suitable for trans-skull sonications. Neuroimage. 2005; 24:12–20. [PubMed: 15588592]
15. McDannold N, Vykhodtseva N, Raymond S, Jolesz FA, Hynynen K. MRI-guided targeted blood-brain barrier disruption with focused ultrasound: histological findings in rabbits. Ultra-sound Med. Biol. 2005; 31:1527–1537.
16. Hynynen K, McDannold N, Vykhodtseva N, Raymond S, Weissleder R, Jolesz FA, Sheikov N. Focal disruption of the blood-brain barrier due to 260-kHz ultrasound bursts: a method for molecular imaging and targeted drug delivery. J. Neurosurg. 2006; 105:445–454. [PubMed: 16961141]
17. McDannold N, Vykhodtseva N, Hynynen K. Targeted disruption of the blood-brain barrier with focused ultrasound: association with cavitation activity. Phys. Med. Biol. 2006; 51:793–807. [PubMed: 16467579]
18. Sheikov N, McDannold N, Jolesz F, Zhang YZ, Tam K, Hynynen K. Brain arterioles show more active vesicular transport of blood-borne tracer molecules than capillaries and venules after focused ultrasound-evoked opening of the blood-brain barrier. Ultrasound Med. Biol. 2006; 32:1399–1409. [PubMed: 16965980]
19. Choi JJ, Pernot M, Small S, Konofagou EE. Feasibility of transcranial, localized drug-delivery in the brain of Alzheimer's-model mice using focused ultrasound. IEEE Int. Ultrasonics Symposium Proceedings. 2005:988–991.
20. Choi JJ, Pernot M, Small S, Konofagou EE. Noninvasive Blood-Brain Barrier Opening in Live Mice. AIP Conference Proceedings. 2006; 829:271–275.
21. Choi JJ, Pernot M, Brown TR, Small SA, Konofagou EE. Spatio-temporal analysis of molecular delivery through the blood-brain barrier using focused ultrasound. Phys. Med. Biol. 2007; 52:5509–5530. [PubMed: 17804879]
22. Choi JJ, Pernot M, Small SA, Konofagou EE. Noninvasive, transcranial and localized opening of the blood-brain barrier using focused ultrasound in mice. Ultrasound Med. Biol. 2007; 33:95–104. [PubMed: 17189051]
23. Konofagou, EE.; Choi, JJ.; Baseri, B.; Lee, A. Characterization and Optimization of Trans-Blood-Brain Barrier Diffusion *In Vivo*. Proceedings of the 8th International Symposium on Therapeutic Ultrasound; Minneapolis, MN, USA. 2009; p. 418-422.
24. Choi JJ, Wang S, Brown TR, Small SA, Duff KE, Konofagou EE. Noninvasive and transient blood-brain barrier opening in the hippocampus of Alzheimer's double transgenic mice using focused ultrasound. Ultrason Imaging. 2008; 30:189–200. [PubMed: 19149463]

25. Konofagou, EE.; Choi, JJ. Ultrasound-induced treatment of neurodegenerative diseases across the blood-brain barrier In: Biomedical Applications of Vibration and Acoustics in Therapy.. In: Al-Jumaily, A.; Fatemi, M., editors. Bioeffects and modelling. ASME Press; New York, NY: 2008. p. 63-80.
26. Choi JJ, Wang S, Tung Y-S, Morrison B III, Konofagou EE. Molecules of various pharmacologically-relevant sizes can cross the ultrasound-induced blood-brain barrier opening *in vivo*. Ultrasound Med. Biol. 2010; 36(1):58–67. [PubMed: 19900750]
27. Baseri B, Choi JJ, Tung YS, Konofagou EE. Safety assessment of blood-brain barrier opening using focused ultrasound and definity microbubbles: a short-term study. Ultras. Med. Biol. 2010; 36(9):1445–1459.
28. Kaufmann BA, Wei K, Lindner JR. Contrast echocardiography. Curr. Probl. Cardiol. 2007; 32:51–96. [PubMed: 17208647]
29. Christensen, D. A. Ultrasonic Bioinstrumentation. John Wiley & Sons; New York: 1988.
30. Miller DL. Overview of experimental studies of biological effects of medical ultrasound caused by gas body activation and inertial cavitation. Prog. Biophys. Mol. Biol. 2007; 93:314–330. [PubMed: 16989895]
31. Chen S, Kroll MH, Shohet RV, Frenkel P, Mayer SA, Gray-burn PA. Bioeffects of myocardial contrast microbubble destruction by echocardiography. Echocardiagraphy. 2002; 19:495–500.
32. Li P, Armstrong WF, Miller DL. Impact of myocardial contrast echocardiography on vascular permeability: Comparison of three different contrast agents. Ultrasound Med. Biol. 2004; 30:83–91. [PubMed: 14962612]
33. Li P, Cao LQ, Dou CY, Armstrong WF, Miller D. Impact of myocardial contrast echocardiography on vascular permeability: An *in vivo* dose response study of delivery mode, pressure amplitude and contrast dose. Ultrasound Med. Biol. 2003; 29:1341–1439. [PubMed: 14553812]
34. Kaps M, Seidel G, Algermissen C, Gerriets T, Broillet A. Pharmacokinetics of echocontrast agent infusion in a dog model. J. Neuroimag. 2001; 11:298–302.
35. Liu P, Gao Y, Tan K, Zhu X, Liu Z, Li P, Narula J, Vannan MA. Impact of Microbubble enhanced Ultrasound on Blood-Brain Barrier Permeability: An *in vivo* dose response study of ultra-sound intensity and contrast dose. Circulation. 2005; 112:U602–U605.
36. Yang FY, Fu WM, Yang RS, Liou HC, Kang KH, Lin WL. Quantitative evaluation of focused ultrasound with a contrast agent on blood-brain barrier disruption. Ultrasound Med. Biol. 2007; 33:1421–1427. [PubMed: 17561334]
37. Miller D, Li P, Dou C, Gordon D, Edwards CA, Armstrong WF. Influence of contrast agent dose and ultrasound exposure on cardiomyocyte injury induced by myocardial contrast echocardiography in rats. Radiology. 2005; 237:137–143. [PubMed: 16183929]
38. Christiansen J, French BA, Klibanov AL, Kaul S, Lindner JR. Targeted tissue transfection with ultrasound destruction of plasmid-bearing cationic microbubbles. Ultrasound Med. Biol. 2003; 29:1759–1767. [PubMed: 14698343]
39. Chomas JE, Dayton P, May D, Ferrara K. Threshold of fragmentation for ultrasonic contrast agents. J. Biomed. Opt. 2001; 6:141–150. [PubMed: 11375723]
40. Borden M, Kruse D, Caskey CF, Zhao S, Dayton PA, Ferrara KW. Influence of lipid shell physicochemical properties on ultrasound-induced microbubble destruction. IEEE Trans Ultrason Ferroelecter. Freq. Control. 2005; 52:1992–2002.
41. Iadecola C. Neurovascular regulation in the normal brain and in Alzheimer's disease. Nat. Rev. Neurosci. 2004; 5:347–360. [PubMed: 15100718]
42. Ghose A, Viswanadhan VN, Wendoloski JJ. A knowledge-based approach in designing combinatorial or medicinal chemistry libraries for drug discovery. 1. A qualitative and quantitative characterization of known drug databases. J. Comb. Chem. 1999; 1:55–68. [PubMed: 10746014]
43. Lipinski C. Drug-like properties and the causes of poor solubility and poor permeability. J. Pharmacol. Toxicol. Methods. 2000; 44:235–249. [PubMed: 11274893]
44. Fischer H, Gottschlich R, Seelig A. Blood-brain barrier permeation: molecular parameters governing passive diffusion. J. Membr. Biol. 1998; 165:201–211. [PubMed: 9767674]
45. Blasberg R, Patlak C, Fenstermacher JD. Intrathecal chemo-therapy brain tissue profiles after ventriculocisternal perfusion. J. Pharmacol. Exp. Ther. 1975; 195:73–83. [PubMed: 810575]

46. Fung L, Shin M, Tyler B, Brem H, Saltzman WM. Chemotherapeutic drugs released from polymers distribution of 1,3-bis(2-chloroethyl)-1-nitrosourea in the rat brain. Pharm. Res. 1996; 13:671–682. [PubMed: 8860421]
47. Pardridge WM. Drug targeting to the brain. Pharm. Res. 2007; 24:1733–1744. [PubMed: 17554607]
48. Neppiras EA. Acoustic cavitation. Phys. Rep. 1980; 61:159–251.
49. Leighton, T. The Acoustic Bubble. First ed.. Academic; London: 1994.
50. Choi, JJ.; Feshitan, JA.; Wang, S.; Tung, Y-S.; Baseri, B.; Borden, MA.; Konofagou, EE. The Dependence of the Ultrasound-Induced Blood-Brain Barrier Opening Characteristics on Microbubble Size *In Vivo*. Proceedings of the 8th International Symposium on Therapeutic Ultrasound; Minneapolis, MN, USA. 2009; p. 58-62.
51. Choi JJ, Small SA, Konofagou EE. Optimization of Blood-Brain Barrier Opening in Mice using Focused Ultrasound. IEEE Int. Ultrasonics symposium Proceedings. 2006:540–543.
52. Choi JJ, Wang S, Morrison B III, Konofagou EE. Molecular Delivery and Microbubble Dependence Study of the FUS-induced Blood-Brain Barrier Opening *In Vivo*. EEE Int. Ultrasonics Symposium Proceedings. 2007:1192–1195.
53. Kinoshita M, McDannold N, Jolesz FA, Hynynen K. Noninvasive localized delivery of Herceptin to the mouse brain by MRI-guided focused ultrasound-induced blood-brain barrier disruption. Proc. Natl. Acad. Sci. USA. 2006; 103:11719–11723. [PubMed: 16868082]
54. Raymond SB, Treat LH, Dewey JD, McDannold NJ, Hynynen K, Bacskai BJ. Ultrasound enhanced delivery of molecular imaging and therapeutic agents in Alzheimer's disease mouse models. PLoS ONE. 2008; 3:e2175. [PubMed: 18478109]
55. Sheikov N, McDannold N, Sharma S, Hynynen K. Effect of focused ultrasound applied with an ultrasound contrast agent on the tight junctional integrity of the brain microvascular endothelium. Ultrasound Med. Biol. 2008; 34(7):1093–1104. [PubMed: 18378064]
56. Treat LH, McDannold N, Vykhodtseva N, Zhang Y, Tam K, Hynynen K. Targeted delivery of doxorubicin to the rat brain at therapeutic levels using MRI-guided focused ultrasound. Int. J. Cancer. 2007; 121:901–907. [PubMed: 17437269]
57. Feshitan JA, Chen CC, Kwan JJ, Borden MA. Microbubble size isolation by differential centrifugation. J. Colloid Interface Sci. 2009; 329:316–324. [PubMed: 18950786]
58. Choi JJ, Selert K, Konofagou EE. Enhanced brain molecular delivery using focused ultrasound at short pulse lengths and low acoustic pressures. IEEE International Ultrasonics Symposium Proceedings. 2010:1518–1521.
59. Farny CH, Holt RG, Roy RA. Temporal and spatial detection of HIFU-induced inertial and hot-vapor cavitation with a diagnostic ultrasound system. Ultrasound Med. Biol. 2009; 35:603–615. [PubMed: 19110368]
60. Tung Y, Choi J, Baseri B, Konofagou EE. Identifying the Inertial Cavitation Threshold and Skull Effects in a Vessel Phantom Using Focused Ultrasound and Microbubbles. Ultras. Med. Biol. 2010; 36(5):840–852.
61. Vlachos F, Tung YS, Konofagou EE. Permeability assessment of the focused ultrasound-induced blood-brain barrier opening using dynamic contrast-enhanced MRI. Phys. Med. Biol. 2010; 55:5451–5466. [PubMed: 20736501]
62. Deffieux T, Konofagou EE. Numerical study and experimental validation of a simple transcranial focused ultrasound system applied to blood-brain barrier opening. IEEE Ultras. Ferroelectr. Freq. Control. 2010; 57(12):2637–2653.
63. Baseri B, Choi JJ, Deffieux T, Samiotaki G, Tung Y-S, Olumolade O, Small SA, Morrison B III, Konofagou EE. Activation of signaling pathways following localized delivery of systemically administered neurotrophic factors across the blood– brain barrier using focused ultrasound and microbubbles. Phys. Med. Biol. 2012; 57:N65–N81. [PubMed: 22407323]
64. Tung Y-S, Vlachos F, Feshitan J, Borden MA, Konofagou EE. the Mechanism of the interaction between focused ultrasound and microbubbles in blood-brain barrier opening in mice. J. Acous. Soc. Amer. 2011; 108130(40)(5):3059–3067.

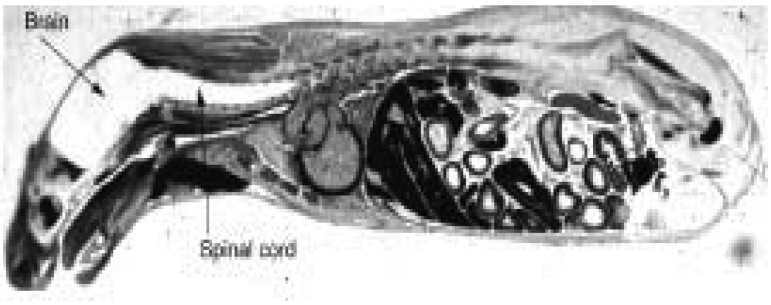

Fig. (1).

Autoradiogram of an adult mouse sacrificed 30 min after intravenous injection of radiolabeled histamine, a small molecule that readily enters all organs of the body, except the brain and spinal cord, as detected by their lack of contrast (Adapted from [4]).

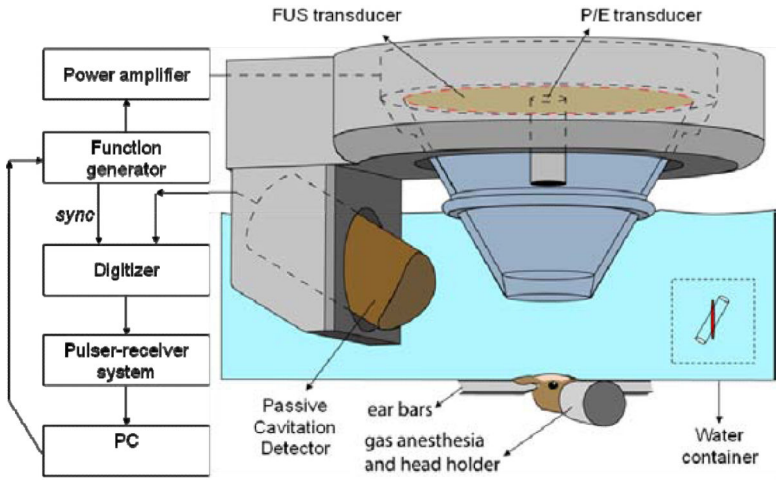

Fig. (2).

Block diagram and illustration of the experimental setup. The PCD was positioned at 60° relative to the longitudinal axis of the FUS beam. The overlap between the focal regions of PCD (blue) and FUS (red) occurring inside the murine brain is illustrated in the inset.

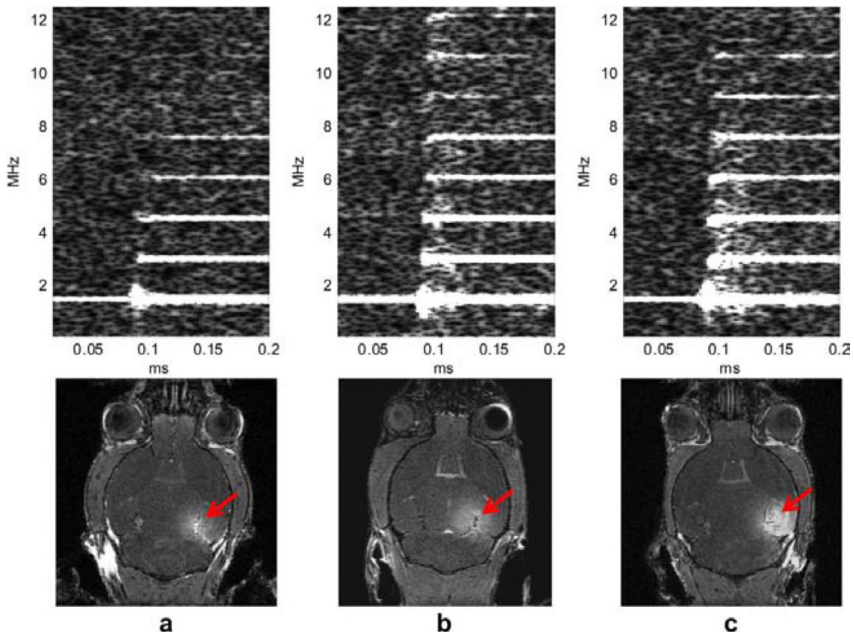

Fig. (3).

Spectrogram during the first 0.2 ms sonication. Broadband acoustic emissions were detected at (b) 0.45 MPa and (c) 0.60 MPa but not at (a) 0.30 MPa. Corresponding MRI images confirm that the blood-brain barrier (BBB) could be opened at 0.30 MPa, i.e., without inertial cavitation. The red arrows indicate the location of BBB opening [60].

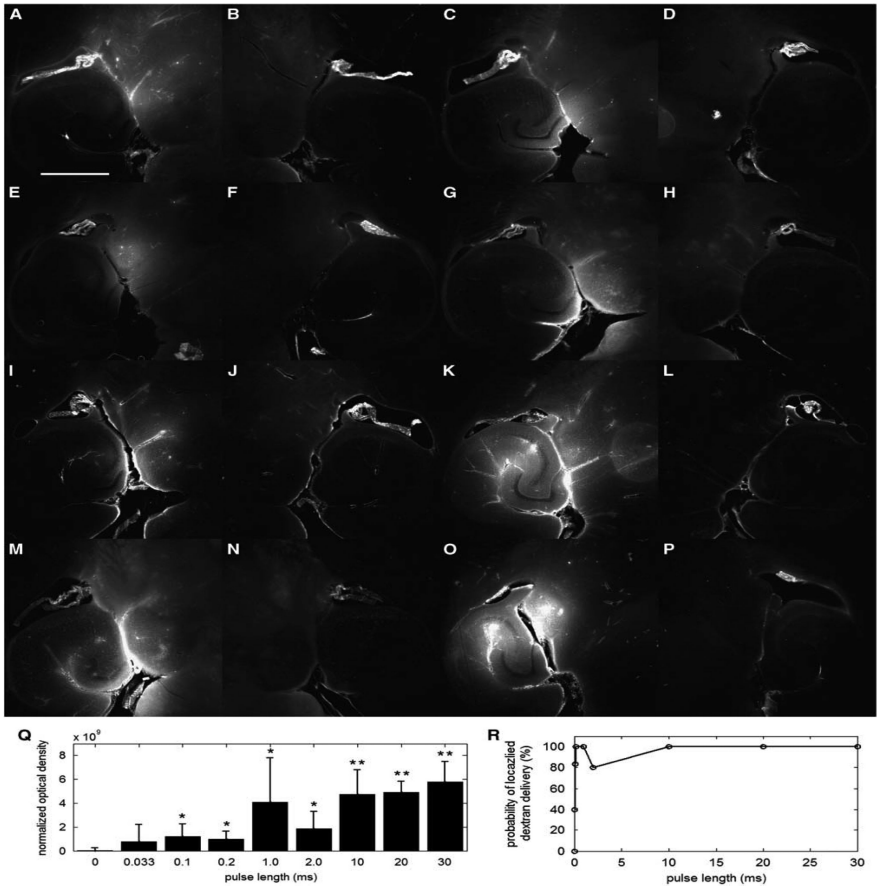

Fig. (4).

Qualitative fluorescence images of the (A, C, E, G, I, K, M, O) left and (B, D, F, H, J, L, N, P) right brain regions of interest (ROI) that have been exposed to pulse length (PL) of (A) 0.033, (C) 0.1, (E) 0.2, (G) 1, (I) 2, (K) 10, (M) 20, and (O) 30 milliseconds. The white scale bar in (A) indicates 1 mm. Quantitative (Q) normalized optical density (NOD) of the left focused ultrasound (FUS)-targeted ROI and (R) probability of localized dextran delivery. The left ROI was sonicated at different PLs. The single asterisk (*) indicates an NOD increase from the sham, whereas the double asterisk (**) indicates a significant increase ($p<0.05$) compared with the 0.033-, 0.1-, and 0.2-millisecond PLs [58].

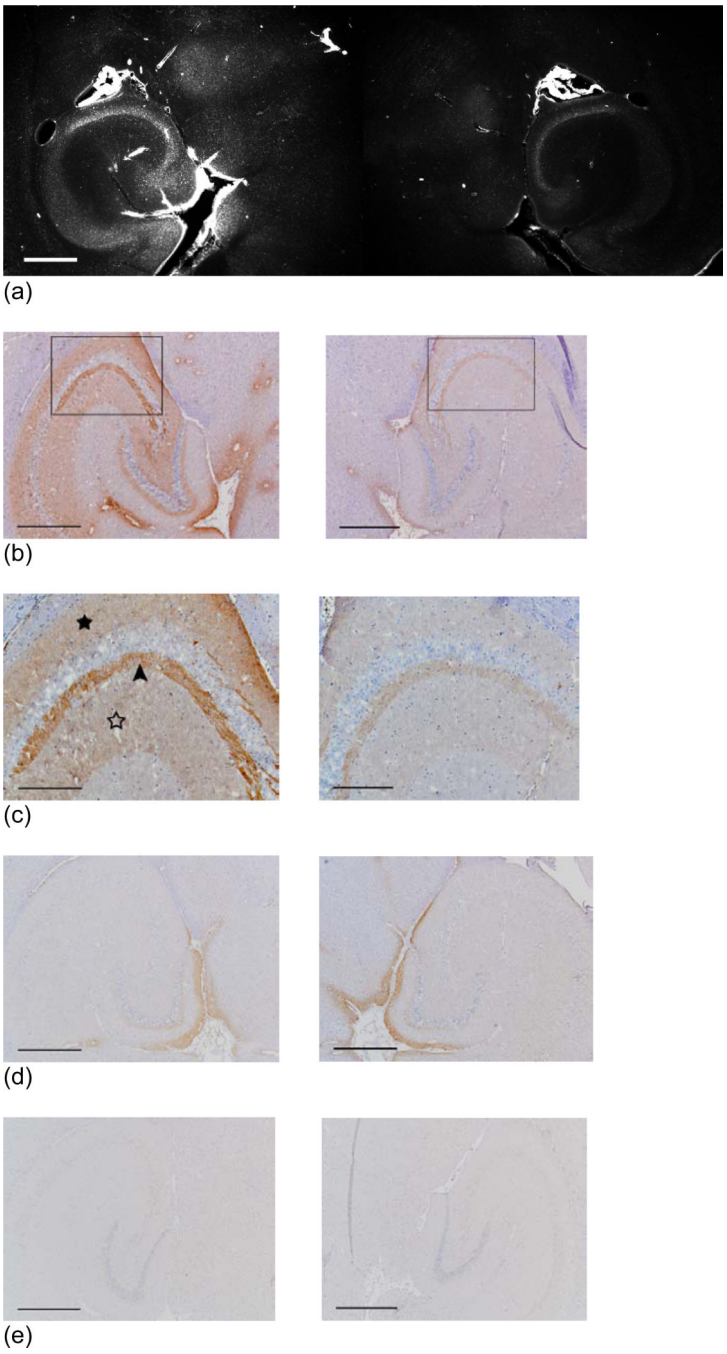

Fig. (5).

Study of the molecular size through the BBB opening using Dextrans and fluorescence imaging: Horizontal slice of Dextran of molecular weight equal to i) 3, ii) 70 and iii) 2000 kDa on the **a**) left (targeted) and **b**) right (not targeted) hippocampus; iv) Coronal slice of the entire brain at 70 kDa Dextran showing the fluorescent left hippocampus (crescent-shaped); v) Fluorescent albumin (67 kDa) permeated in the putamen through the opened BBB.

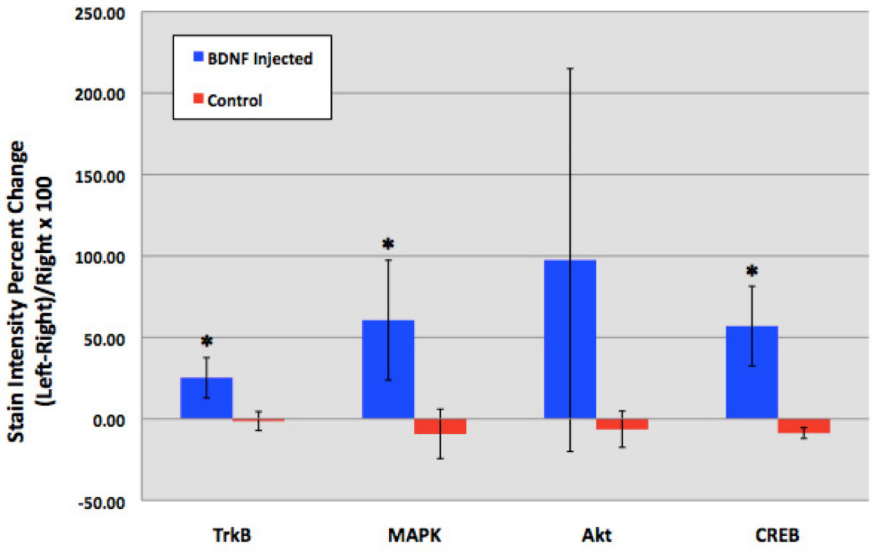

(f)

Fig. (6).

Comparison between MRI (left) and histology (center (1x) and right (200x near the region of most enhanced BBB opening according to the MRI) after FUS-induced BBB opening on the left hippocampus at **i**) 0.45 and **ii**) 0.75 MPa peak rarefactional pressure. It shows that at lower pressures ((**i**)) the endothelial and neurons are intact (red) while at higher pressures ((**ii**)) there is extravasation of red blood cells (indicated by arrowhead) and neuronal death (indicated by arrow). This indicates the safety window of the FUS technique in BBB opening.

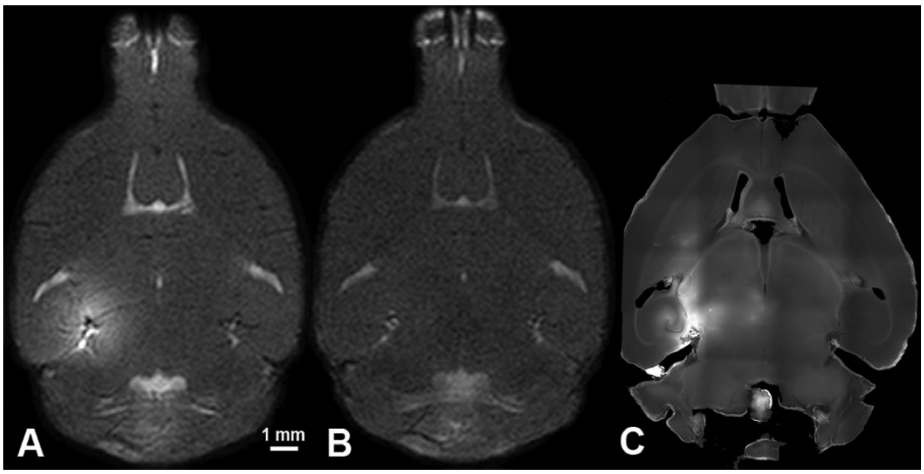

Fig. (7).

T1 MRI images of **A**) BBB opening, **B**) BBB closing (24 hours); and **C**) fluorescence imaging with 3-kDa dextran of the left (sonicated hippocampus).

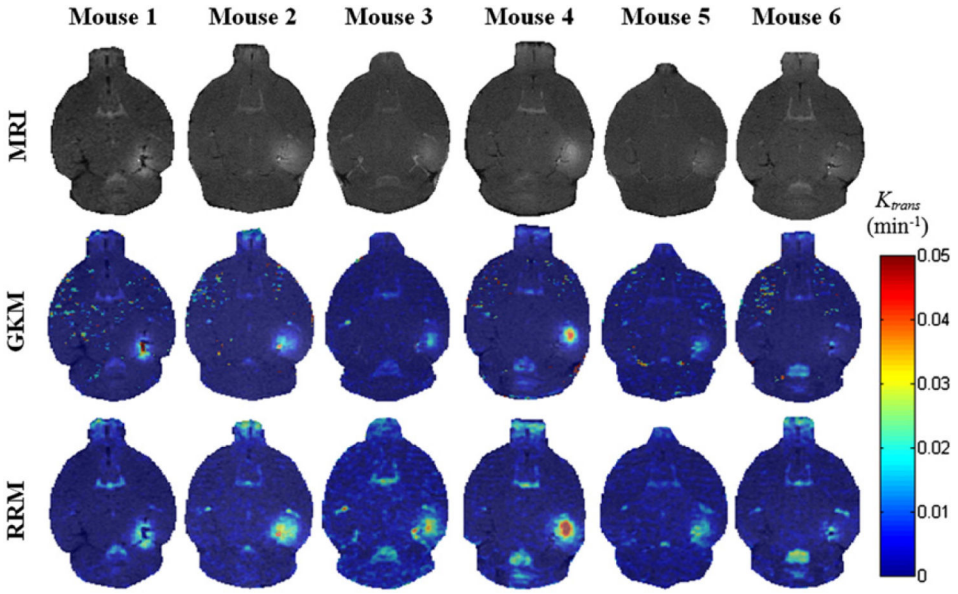

Fig. (8).

T1 images (first row) and their corresponding permeability maps generated from two different kinetic models, GKM (second row) and RRM (third row) for all mice. The transverse slice with maximum T1 signal enhancement is selected. The Ktrans values are indicated in the colorbar. The maps have been superimposed over the corresponding DCE-MR images. In the case of mouse 1, the last acquired DCE-MR image is presented instead of a regular T1 [61].

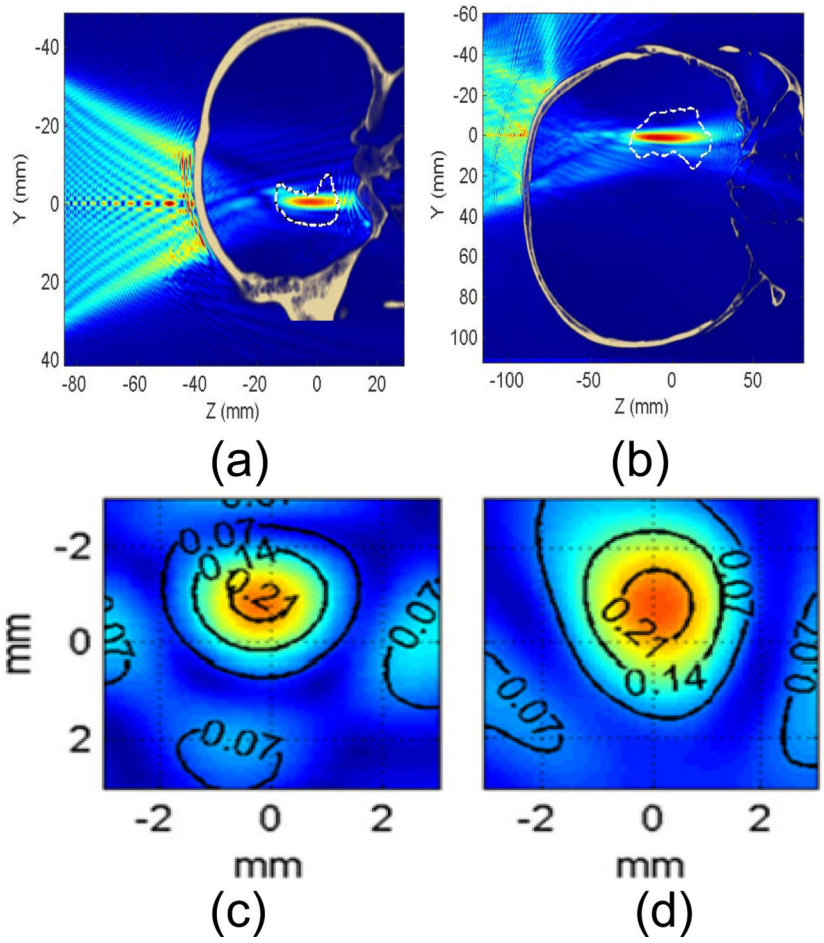

Fig. (9).

Theoretical simulations with experimental validation for predicting the area of BBB opening (in red) relative to the hippocampus (white dashed contour through the skull) of **a**) non-human primates at 800 kHz and **b**) human at 500 kHz. In both cases, there is formation of a uniform focal spot with the largest dimension along the longest dimension of the hippocampus in both cases. **c**) Experimental validation of a uniform focal spot (transverse view) through the *ex vivo* primate skull of the **d**) simulated focal spot at 800 kHz [62].

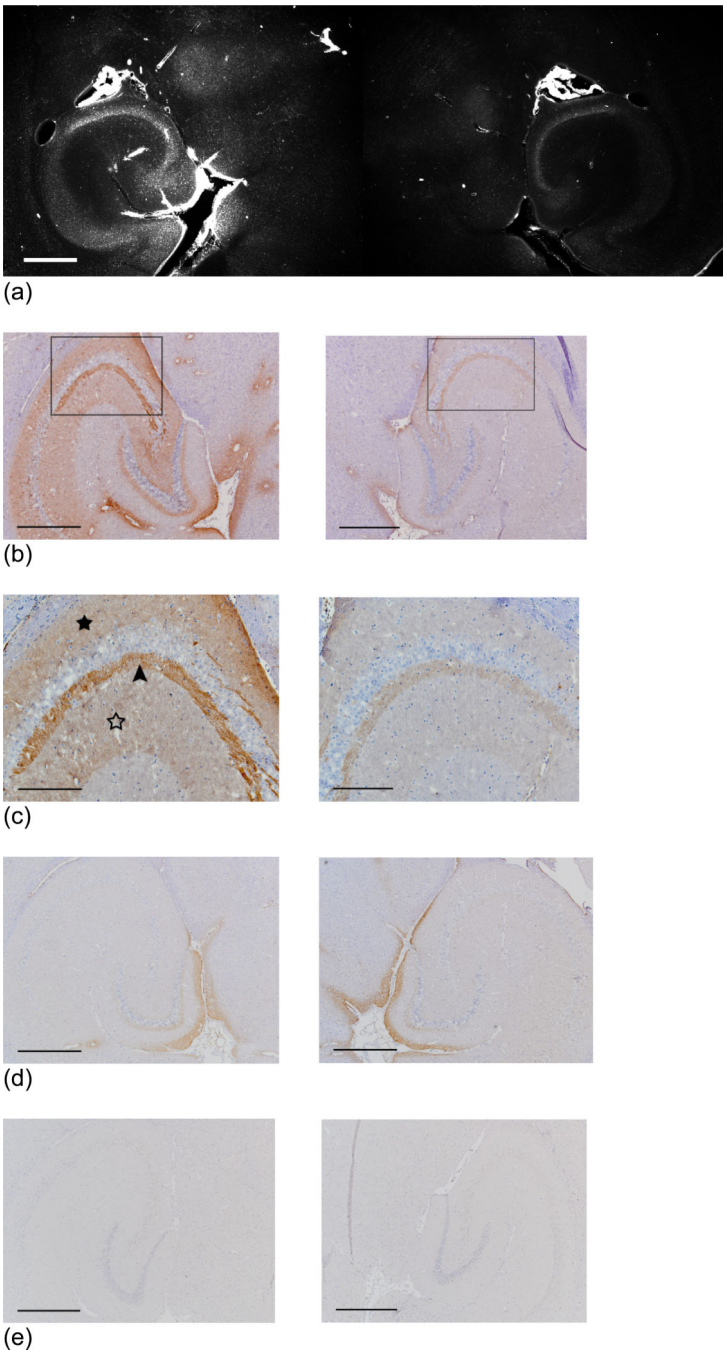

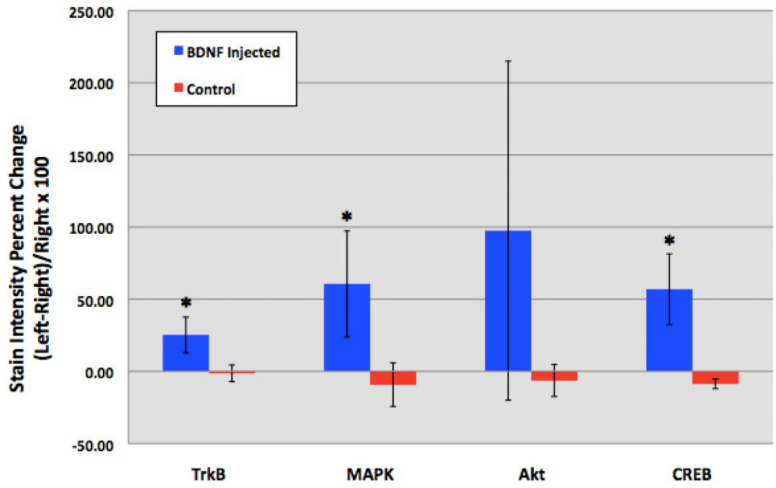

Fig. (10).

(**a**) Fluorescent image of a 100-micron frozen brain section from a mouse that was sacrificed 20 min after sonication. The sonicated hippocampus (left) shows much higher fluorescent intensity than the un-sonicated hippocampus (right), depicting blood-brain barrier opening and the extravasation of fluorescent-tagged (Alexa Fluor 594) BDNF in the sonicated region; (**b**) a 5-micron frozen section from the same mouse was immunohistochemically stained using a primary antibody against phosphorylated MAPK (pMAPK). Consistent with the fluorescent image in (**a**), the intensity of DAB staining is much greater in the left sonicated hippocampus compared to the right control; the black box shows the enlarged area in (**c**), where immunoreactivity to pMAPK is shown in mossy fiber terminals (arrowhead), suprapyramidal CA3 dendrites (black star), and the axons of the Schaffer collateral system (hollow star); (**d**) immunohistochemical staining of a 5-micron frozen section from a mouse that was sacrificed 3 min after sonication; the same primary antibody against pMAPK was used. No difference in DAB intensity is observed between the sonicated and the control hippocampus; (**e**) Negative control for the same mouse in (**a**); no primary antibody (against pMAPK) was added to this 5-micron frozen section during the staining procedure. All magnifications are 40x and scale bars are 500 μm except for (**c**), which is 100x and 200 μm, respectively. In (**f**), immunohistology stain intensity analysis shows percentage change between the left (FUS) and the right (no FUS) sides of the mice brains. A significant difference ($p<0.05$, N=3; depicted by asterisks) was found between the BDNF administered animal group and the control (no BDNF) animal group for the TrkB, MAPK, and CREB antibodies. Bars represent mean ± standard deviation [63].

Table 1

Clinically Used Contrast Agents and their Specifications

Formulation (Manufacturer)	Shell/Gas	Concentration (ml^{-1})	Mean Diameter (μm)	Gas Volume Fraction[$]	Dose (ml/kg)
Optison (GE Healthcare)	Albumin/C_3F_8	8×10^8	3.0-4.5	1.1-3.8%	0.006-0.1[*]
Definity (Bristol-Myers Squib)	Lipid/C_3F_8	1.2×10^{10}	1.1-3.3	0.8-23%	0.01-0.02[**]
Sonovue (Bracco)	Lipid/SF_6	2×10^8	2.5	0.2%	0.003-0.3[**]

[$] Determined from concentration and mean diameter.

[*] Data obtained from Optison package insert.

[**] Data from NIH Molecular Imaging and Contrast Agent Database (MIDAC).

Table 2

Techniques Shown to Induce trans-BBB Transport or BBB Disruption

Method	Description	Problems	Non-Invasive?	Localized?
Lipidization	"Lipidize" the drug. Allows uptake in the BBB.	Increases penetration across *all* biological membranes.	Yes	No
Transcranial brain drug delivery	Neurosurgically-based drug delivery method. Diffusion-based method.	Invasive. Diffusion reduces the initial concentration by 90% when traveling only 0.5 mm.	No	Yes
Solvent/adjuvant-mediated BBB disruption	Solvent and adjuvants disrupt the BBB using dilation, contraction, and other methods.	Disrupts the BBB in all of the brain. Potentially toxic.	Yes	No
Delivery through endogenous transporters	Use endogenous transporters to traverse the BBB.	Requires medicinal chemistry to modify drugs and knowledge of the endogenous transporters.	Yes	No
Ultrasound	Focused Ultrasound (FUS) with microbubbles	Possible irreversible damage may be induced.	Yes	Yes